EFFECTS OF VERTICAL PLATES ON THE UNSTEADY PRESSURE CHARACTERISTICS OF RECTANGULAR CYLINDERS

Cristiano Augusto Trein[+1], Hiromichi Shirato[+2], Masaru Matsumoto[+3]

[1,2,3]Department of Civil and Earth Resources Engineering, Kyoto University, Kyoto, Japan

ctrein@cristianotrein.com, shirato@brdgeng.gee.kyoto-u.ac.jp, matsu@brdgeng.gee.kyoto-u.ac.jp

This study investigates the effects of vertical plates on the unsteady pressure characteristics of rectangular cylinders. Effects on phase difference distributions appear as a negative jump at plate's location, followed by a recovering tendency. As for amplitude distributions, two peaks are observed; one at plate's location, another in its downstream. The magnitudes of peaks and jumps are related to size of plate and its distance from leading edge. A peculiar behavior is identified in configurations with two vertical plates. The unsteady pressure characteristics of such arrangements result from a superposition of the effects obtained separately from the corresponding single plates configurations.

Keyword: flutter, unsteady pressure characteristics, fairing, vertical plate, rectangular cylinder, wind tunnel experiment.

1. INTRODUCTION

Aerodynamic instabilities have been of major concern in the design of modern long-span bridges. As spans get longer, decks get slender and fluid-structure interactions get more important. In this scenario, flutter instability has drawn the attention of the scientific and engineering communities. The present investigation is inserted in this context. Motivated by flutter stabilization efforts, experimental studies on rectangular cylinders equipped with vertical plates at different locations are developed. The objective is to clarify relationships between flutter and deck geometry towards the development of methods for flutter stabilization in long-span bridges.

Because aerodynamic interactions are very complex, every new arrangement of cross-section has to be investigated from scratch, resulting in repetitive costs and time consumption. In practical terms, investigations have focused on finding relationships between geometry and flutter stabilization, through the control of aerodynamic derivatives. The goal has been to lead aerodynamic derivatives to stable configurations. In this sense, relationships between geometry and aerodynamic derivatives have been proposed. However, such relationships are very complex and no universal rule has been achieved so far.

Based on such investigations, some guidelines for flutter stabilization have been accepted as common sense among bridge designers. The most important of them refers to the stabilizing role played by negative values of A_2^* derivative [1;2;3]. Also, A_1^* has been regarded as of relevance in terms of onset velocity. Considering the interdependence between aerodynamic derivatives[4], variations in A_3^* derivative can relate to flutter instabilization as well. Nevertheless, derivatives interdependence holds well only in streamlined cross-sections[5], which means that relying only on them may lead to uncertainties, when it comes to more complex geometries of cross-sections.

Because aerodynamic derivatives can derive from the unsteady pressure characteristics developed along the bridge deck, it must be also possible to face the problem of stability of bridges by considering directly the relationships between geometry and unsteady pressure characteristics. Previous investigations demonstrated that flutter can be stabilized by moving peaks in amplitude distributions to downstream while keeping phase difference distributions within the limits of a stability range[6]. The drawback is that relationships between geometry and unsteady pressure characteristics can be achieved only through time consuming techniques. Because of that, they are scarce in the literature. That is a motivation to propose studies in this sense.

By understanding the effects of every *geometric singularity* (geometric modification such as vertical plates, slots, etc) on the unsteady pressure characteristics, it would be possible to compose unsteady pressure characteristics conveniently for flutter stabilization in a preliminary design stage. By doing so, experimental

[+1]ctrein@cristianotrein.com, [+2]shirato@brdgeng.gee.kyoto-u.ac.jp, [+3]matsu@brdgeng.gee.kyoto-u.ac.jp

procedures would be reserved to more advanced stages in the design process. In this sense, investigations with two-box girders have demonstrated that unsteady pressure characteristics of dowstream boxes are defined mainly by the characteristics of the slot and the geometry of its cross-section itself[7], regardless the upstream box geometric configuration. Moreover, slots were found to cancel effects of vertical plates on the upstream box. Despite non-linearities in terms of aerodynamic derivatives, there were simple patterns in terms of relationships between geometry and usteady pressure characteristics.

Results to be reported herein expand such investigations. Based on studies previously conducted by the authors[7;8;9;10], influences of vertical plates on the unsteady pressure characteristics of rectangular cylinders were investigated. As a result, proportionality relationships between size an location of vertical plates with both amplitude and phase difference distributions are identified. Plates of different sizes at different locations along the body were considered.

2. EXPERIMENTAL SET-UP

Investigations were based on wind tunnel tests of harmonically oscillating models in Kyoto University Bridge Engineering Laboratory. Models consisted of rectangular cylinders with vertical plates of two different sizes disposed on its upper surface at different locations. Pressure distributions were measured and analyzed. Discussions on results focused on the role played by location and size of vertical plates in the formation of unsteady pressure characteristics along the upper surface of the models.

The wind tunnel used in the experiments was a room-circuit Eiffel-type tunnel, with a working section 1.8m in height and 1.0m in width. The base model was a *B/D=20* rectangular cylinder (where *B* is the width and *D* is the thickness) made of wood. Fig.1(a) illustrates the experimental set-up.

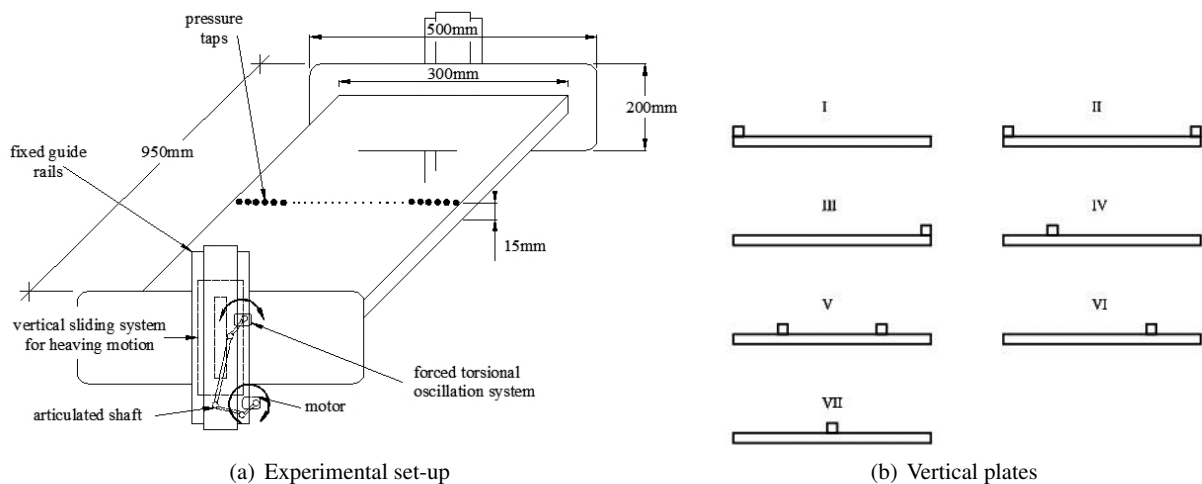| (a) Experimental set-up | (b) Vertical plates |

Figure 1: Models

Vertical plates were made of naval wood with a thickness of 3mm and heights equivalent to $D/2$ and D. They were affixed to the upper surface of the models, according to configurations of Fig.1(b). Models were instrumented with 30 equidistant pressure taps, placed on their upper surface, along the chordwise direction at the center of their spans. Pressure measurements were performed in a smooth flow, with turbulence less than 0.5%, via the forced heaving/torsional 1-DOF (degree of freedom) oscillation method. For both motions, frequency of forced oscillation was set to f=2Hz. Amplitude of oscillation in torsional system was $2\varphi_0$=4°; in heaving system, amplitude was $2\eta_0$=20mm. Reduced wind velocities, defined by $U/f.B$ (where U is the wind velocity), ranged from $U/f.B = 5$ to $U/f.B = 25$, in steps of 5.

In the analysis of pressure distributions in harmonically oscillating bodies, information is discretized according to the non-dimensionalized (normalized by the half width b) x widthwise coordinate. This parameter is defined as x^* and ranges from -1 to $+1$, where 0 is the center of the cross-section. For every normalized location x^*, pressure signals are divided into mean and fluctuating pressure components. In this study, discussions are restricted to fluctuating pressure components, which correspond to the so-called *unsteady pressure characteristics*.

The equation below describes the fluctuation pressure components.

$$\tilde{C}_p(x^*, t) = -\tilde{C}_p(x^*) . cos(2.\pi.f.t - \psi(x^*))$$

(1)

where $\tilde{C}_p(x^*, t)$ is the fluctuating pressure coefficient at x^* at time t; $\tilde{C}_p(x^*)$ is the full amplitude (negative to positive peaks) of the unsteady pressures, normalized by the dynamic pressure of the flow $1/2.\rho.U^2$; ρ is the air density; f is the forced oscillation frequency; t is the time; $\psi(x^*)$ is the phase difference between the maximum relative angle of attack of the model and the negative pressure peak on its upper surface at every location x^*.

Models are identified by a composition of the code of the regular *B/D=20* rectangular cylinder (*NF*), the set-up code (Fig.1(b)) and the size code of the vertical plates, which is *A* for height=D/2 and *B* for height=D.

3. EXPERIMENTAL RESULTS

Rectangular cylinders have been widely used as fundamental geometries in investigations on bridge decks. Because of that, a large amount of data regarding such a cross-section is available in literature. In order to profit from such a database, a rectangular cylinder was chosen for this investigation. The decision for a large side ratio (B/D=20) was based on the current tendency modern bridges have experienced towards slender decks.

In rectangular cylinders, remarkable similarities between unsteady pressure characteristics obtained from heaving and torsional forced oscillations have been identified[4]. However, in bridge decks, this phenomenon has shown dependence on the shape of the cross-section. Studies have demonstrated that the similarity between torsional and heaving systems in bridge decks decreases with the increase of the complexity of the deck geometry[11;12;13]. Such an effect has a great impact on the aerodynamic derivatives, especially on the interdependence mentioned in the Introduction. Consequently, flutter stability itself is also affected. The understanding of how modifications in geometry can exert influence on such a break of similarity is a factor to be understood to control flutter stabilization from the unsteady pressure characteristics point of view.

Results of investigations are organized according to set-ups and sizes of vertical plates. They are accompanied by considerations on the relationships of size and location of the vertical plates with the resulting impacts on phase difference $\psi(x^*)$ and amplitude $\tilde{C}_p(x^*)$ distributions. The results may be also considered as an assessment of the effects of separation points and blockages along the chord direction in the upper surface of rectangular cylinders. Fig.2 presents the unsteady pressure characteristics for the B/D=20 rectangular cylinders (model *NF*). The following sections present other results.
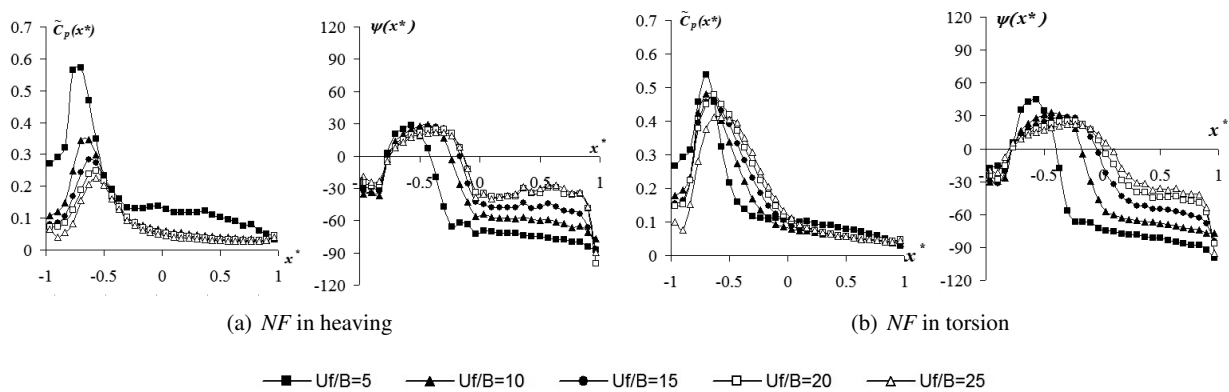

(a) *NF* in heaving

(b) *NF* in torsion

—■— Uf/B=5   —▲— Uf/B=10   —●— Uf/B=15   —□— Uf/B=20   —△— Uf/B=25

Figure 2: Unsteady pressure characteristics of B/D=20 rectangular cylinder

(1) Vertical plate at the leading edge

Fig.3 reports the experimental data obtained by installing vertical plates of two different sizes at the leading edge. For both plates, amplitude $\tilde{C}_p(x^*)$ distributions resemble those obtained for a regular $B/D = 20$ rectangular cylinder (Fig.2). However, a shift downstream of the peak is observed with the increase of the size of the plate. Techniques of flow visualization combined with pressure measurements have pointed out that the location of the peak of the fluctuating pressures in stationary rectangular cross sections is related to the reattachment of the separated flow, revealing the dimension of the separation bubble[14]. This location was found

to be in a distance $x_0^* = 4.4D/b$ from the leading edge. Even though this relationship refers to stationary cylinders, peaks in the distributions of Fig.2 at the highest reduced wind velocity (*U/f.B=25*) were situated within that limit.
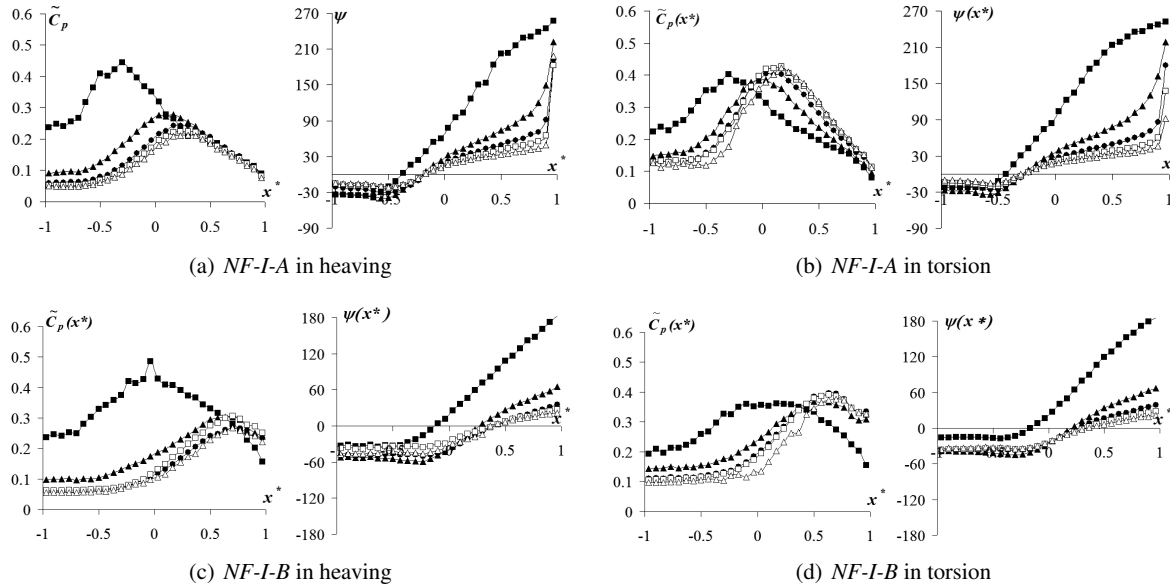

(a) *NF-I-A* in heaving

(b) *NF-I-A* in torsion

(c) *NF-I-B* in heaving

(d) *NF-I-B* in torsion

Figure 3: Unsteady pressure characteristics of B/D=20 rectangular cylinders with vertical plates *A* and *B* at the leading edge

It was so attempted to check whether the relationship above could be applied to the results of Fig.3. Even though the original relationship was obtained with stationary models and results presented herein related to models in harmonic motion, such comparison may provide an insight for the definition of semi-empirical relationships to be used in investigations with rectangular cylinders.

The distances x_0^* between the leading edge and the peaks of all $\tilde{C}_p(x^*)$ distributions of Fig.3 were used in the calculation of an *equivalent thickness* D_{eq} that would satisfy the equality $x_0^* = 4.4.D_{eq}/b$. From this *equivalent thickness* D_{eq}, an *equivalent side ratio* BD_{eq} was calculated. In this context, another convenient parameter is the *apparent side ratio* $(B/D)_{ap}$. This index is defined as a ratio between width B of the original rectangular cross-section and the resulting cross-flow dimension, which is composed of the actual thickness D of the cylinder and the height of the vertical plate. Results are reported in Table 1.

Table 1: Equivalent side ratio, equivalent thickness and apparent side ratio for *NF-I-A* and *NF-I-B*, calculated through $x_0^* = 4.4D_{eq}$

U/f.B	5		10		15		20		25		$(B/D)_{ap}$
	D_{eq}	BD_{eq}	D_{eq}	BD_{eq}	D_{eq}	BD_{eq}	D_{eq}	BD_{eq}	D_{eq}	BD_{eq}	
NF-I-A in torsion	0.16	12.57	0.23	8.52	0.23	8.52	0.27	7.54	0.27	7.54	13.3
NF-I-A in heaving	0.16	12.57	0.27	7.54	0.30	6.77	0.30	6.77	0.30	6.77	13.3
NF-I-B in torsion	0.27	7.54	0.34	5.87	0.37	5.39	0.37	5.39	0.39	5.18	10.0
NF-I-B in heaving	0.22	9.10	0.37	5.39	0.39	5.18	0.39	5.18	0.39	5.18	10.0

With the increase of the reduced wind velocity, *equivalent side ratios* BD_{eq} tend to values nearly the

half of the *apparent side ratios* $(B/D)_{ap}$. Comparing the amplitude distributions $\tilde{C}_p(x^*)$ of these cases with previous experimental data[4], it is observed that distributions of Fig.3 assume, indeed, configurations similar to the ones related to their *equivalent side ratios* BD_{eq}. Amplitude distribution of *NF-I-A* is in an intermediate state between rectangular cylinders with side ratios B/D=5 and B/D=7.5. Although magnitude of peaks do not show a full concordance, their positions do. Such a comparison can be seen in Fig.4, for *NF-I-A* in torsion. Similar comparison is provided for *NF-I-B* in torsion in Fig.5.
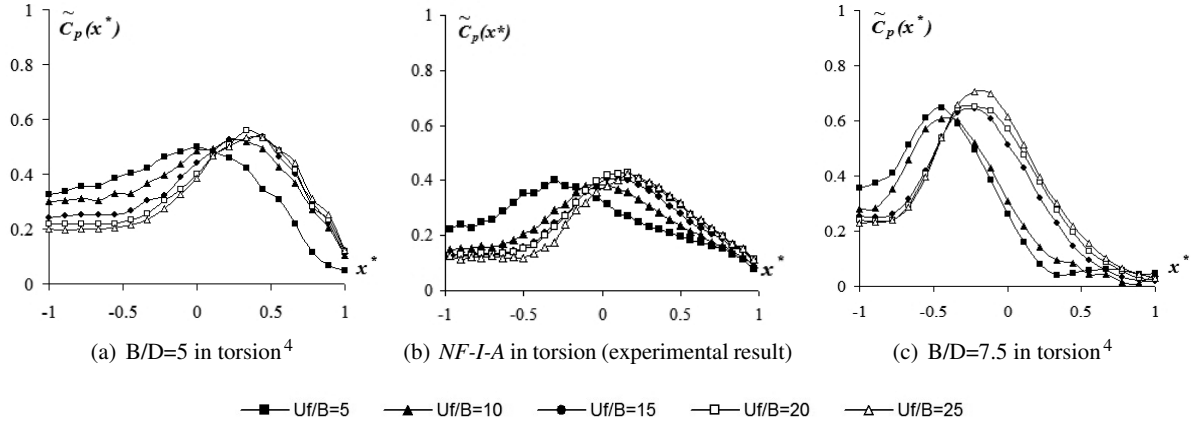

(a) B/D=5 in torsion[4]   (b) *NF-I-A* in torsion (experimental result)   (c) B/D=7.5 in torsion[4]

——■—— Uf/B=5   ——▲—— Uf/B=10   ——●—— Uf/B=15   ——□—— Uf/B=20   ——△—— Uf/B=25

Figure 4: Comparison between amplitude $\tilde{C}_p(x^*)$ distributions of rectangular cylinders with side ratios B/D=5, B/D=7.5 and *NF-I-A*, in torsion

(a) B/D=5 in torsion[4]   (b) *NF-I-B* in torsion (experimental result)

——■—— Uf/B=5   ——▲—— Uf/B=10   ——●—— Uf/B=15   ——□—— Uf/B=20   ——△—— Uf/B=25
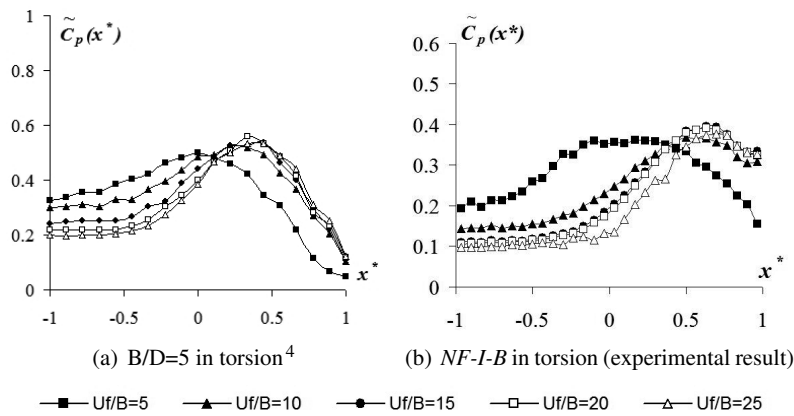
Figure 5: Comparison between amplitude $\tilde{C}_p(x^*)$ distributions of rectangular cylinders with side ratios B/D=5 and *NF-I-B*, in torsion

A vertical plate at the leading edge induces amplitude distributions $\tilde{C}_p(x^*)$ to behave as if it derived from a regular rectangular cylinder with an *equivalent side ratio* 50% smaller than the *apparent side ratio*. Based on that, a comparison link between modified rectangular cylinders (with a vertical plate at the leading edge) and the basic *B/D=20* configuration can be proposed. Relationships in terms of unsteady pressure characteristics might be established from this perspective.

When it comes to phase difference distributions $\psi(x^*)$, a comparison between distributions $\psi(x^*)$ of Fig.3 and Fig.2 shows that a vertical plate at the leading edge promotes a kind of *scale amplification* on the distributions, as if the region near the leading edge is zoomed in. Curves become elongated, which implies in transferring the first crossing point of the x axis to downstream. For a sake o brevity, in Fig.6, a comparison similar to the one of Fig.4 is provided for the phase difference distributions $\psi(x^*)$ of *NF-I-A*. It is shown that the phase difference distributions of *NF-I-A* are comparable to the ones of a rectangular cylinder with side ratio B/D between 5 and 7.5, which is a conclusion similar to the one obtained for the $\tilde{C}_p(x^*)$ distributions.
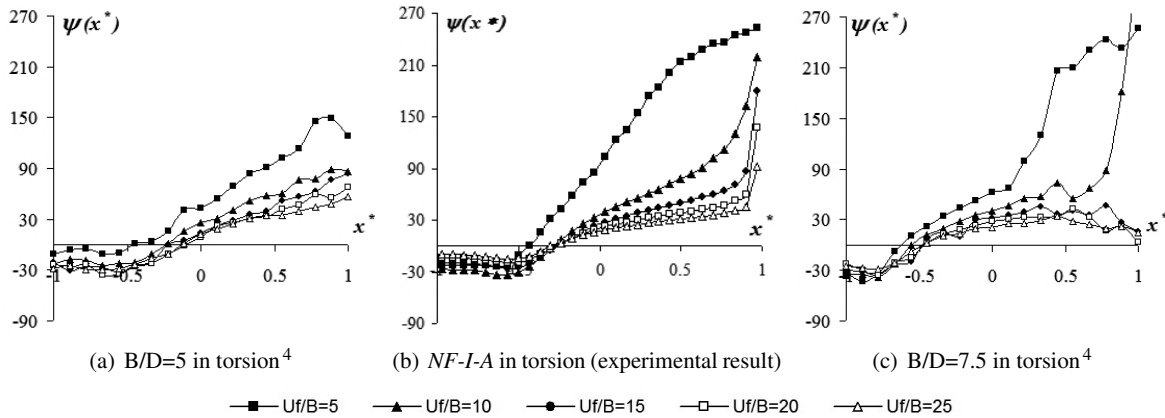
(a) B/D=5 in torsion[4]   (b) *NF-I-A* in torsion (experimental result)   (c) B/D=7.5 in torsion[4]

—■— Uf/B=5   —▲— Uf/B=10   —●— Uf/B=15   —□— Uf/B=20   —△— Uf/B=25

Figure 6: Comparison between phase difference $\psi(x^*)$ distributions of rectangular cylinders with side ratios B/D=5, B/D=7.5 and *NF-I-A*, in torsion

In the phase difference distributions $\psi(x^*)$ of *NF* in Fig.2 ($B/D = 20$), all curves cross x axis almost at the same point x_1^*, which is in a distance $\Delta x^* \simeq 0.22$ from leading edge in torsional system and $\Delta x^* \simeq 0.25$ from leading edge in heaving system. For *NF-I-A*, apart from the lowest reduced wind velocity (*U/f.B=5*), all curves also cross x axis almost at the same point x_1^*: $\Delta x^* \simeq 0.70$ in torsional system and $\Delta x^* \simeq 0.80$ in heaving system. These values keep nearly the same 1/3 proportionality existent between *equivalent side ratio* BD_{eq} and actual side ratios for *B/D=20* model.

Checking the same assumptions for *NF-I-B*, the conclusions are similar. Even though *apparent side ratio* is $(B/D)_{ap} = 10$, *equivalent side ratio* BD_{eq} is induced to present half of this value, Fig.7.

(a) B/D=5 in torsion[4]   (b) *NF-I-B* in torsion (experimental result)

—■— Uf/B=5   —▲— Uf/B=10   —●— Uf/B=15   —□— Uf/B=20   —△— Uf/B=25
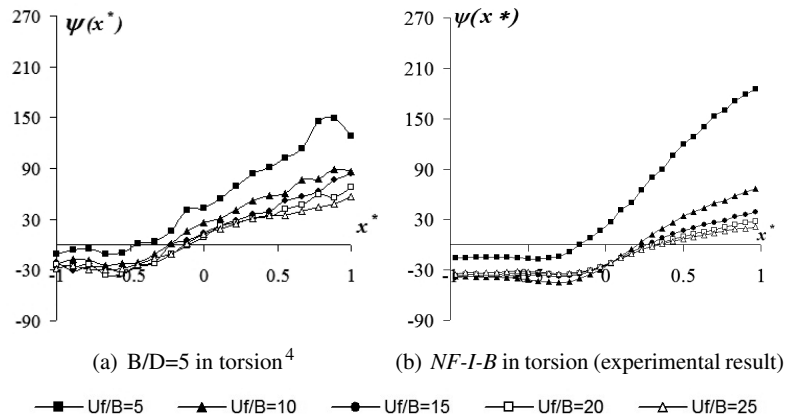
Figure 7: Comparison between phase difference $\psi(x^*)$ distributions of rectangular cylinders with side ratios B/D=5 and *NF-I-B*, in torsion

(2) Single vertical plates of size *A* and *B* along the chord direction

In Fig.8, unsteady pressure characteristics of models with plate of size *A* and *B* installed at three different locations – set-ups *IV*, *VI* and *VII* – are compared with distributions from the configuration without vertical plate (*NF*). For a sake of brevity, only *U/f.B=25* is reported.

Effects of vertical plates are perceived in both upstream and downstream of their locations, in both amplitude and phase difference distributions. Upstream of the vertical plate, flow is blocked. The recirculation created by this blockage increases the level of the fluctuating components of the pressure signal and delays the development of the flow. This is translated into a broadening of the amplitude distributions $\tilde{C}_p(x^*)$ in that region and into the imposition of a positive *bias* on the phase difference distributions $\psi(x^*)$. Positive values of phase difference $\psi(x^*)$ represent a delay in the flow. These effects are perceived throughout all wind velocities range
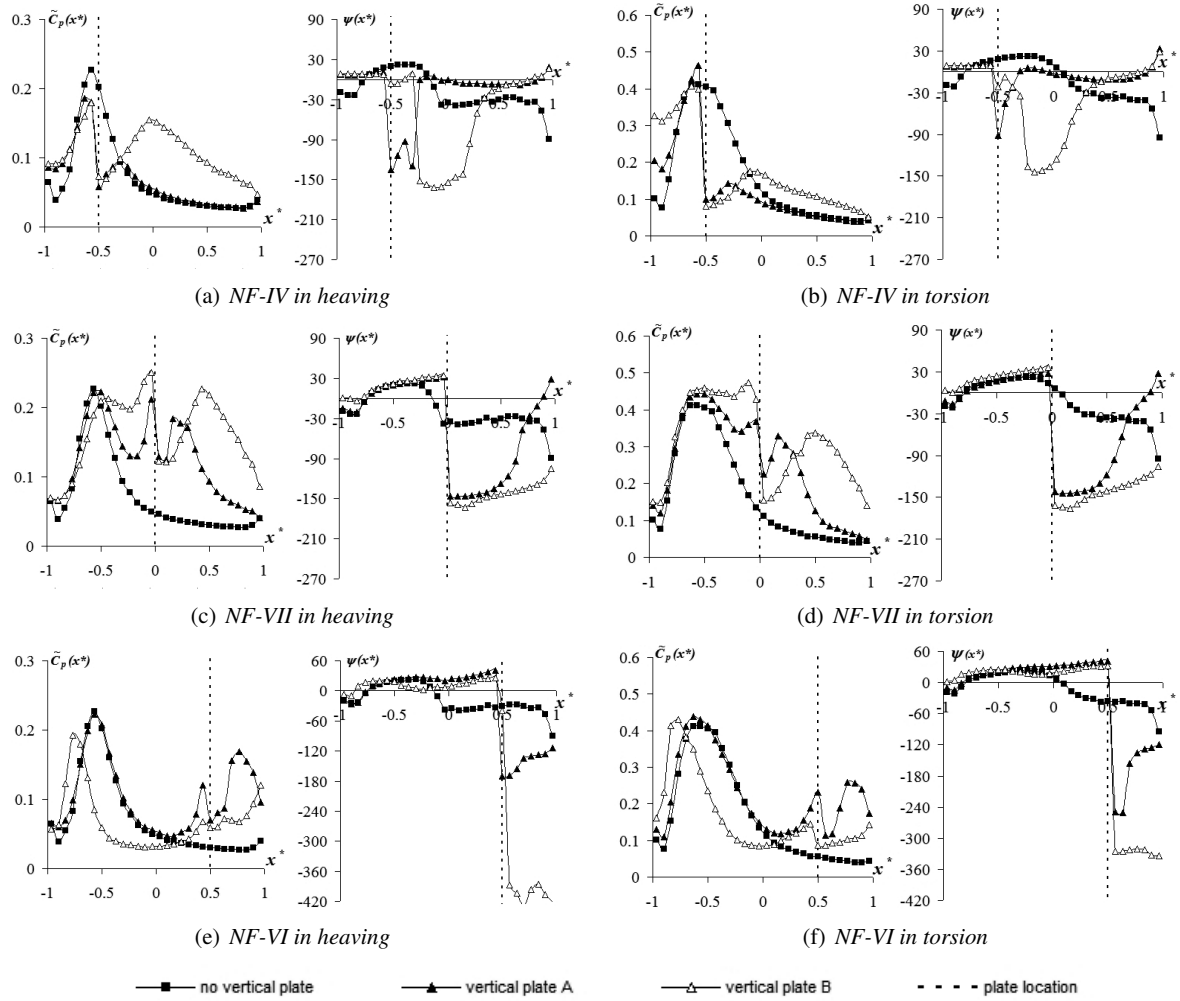
(a) *NF-IV in heaving*

(b) *NF-IV in torsion*

(c) *NF-VII in heaving*

(d) *NF-VII in torsion*

(e) *NF-VI in heaving*

(f) *NF-VI in torsion*

— ■ — no vertical plate   — ▲ — vertical plate A   — △ — vertical plate B   - - - - plate location

Figure 8: Set-ups *IV*, *VII* and *VI*, with plates of size *A* and *B*, superimposed for leading edges *NF* at *U/f.B=25*

and are emphasized with the increase of the velocity.

In amplitude $\tilde{C}_p(x^*)$ distributions, effects are summarized by the presence of two peaks: one at the vertical plate's location and another in its downstream. When the plate is inside the limits of the peak promoted by the leading edge (set-up *IV*), both peaks get superimposed. As vertical plate moves towards trailing edge (set-ups *VII* and *VI*), peaks become separated. The peak due to the leading edge reappears and its corresponding curve develops itself until reaching some point before the vertical plate, where the curve inverts its decaying tendency and goes up towards the peak related to the vertical plate.

At the vertical plate, flow is separated again. A valley is induced, followed by an ascendant tendency towards the second peak. This last peak must be associated to the reattachment of the flow separated by the vertical plate. The values reached by both peaks depend on the location of the plate. In set-up *IV*, the second peak is weaker and located at a shorter distance from the vertical plate, compared to set-ups *VI* and *VII*. This is a consequence of the high vorticity of that region, in a scale larger than the size of the vertical plate. So, the influences of the plate get proportionally reduced.

In set-ups *VI* and *VII*, amplitude distributions $\tilde{C}_p(x^*)$ start the inversion of the decaying tendency (upstream of the vertical plate) at a location nearly symmetric to the location of the peak induced downstream of the plate. Both distances vary with vertical plate's location and size. In heaving system, they tend to be longer than in torsional system. In average, they reach values around $\Delta x^* = 0.3$ in non-dimensional units for set-up *VII − A* and $\Delta x^* = 0.4$ for set-up *VI − B*. These values double for plate *B*. Also, with the increase of size, a slight increase in the values of the peaks is noticed. In set-up *VI − B*, the larger size of plate results in a compression of the

distribution, displacing the first peak to upstream.

As for phase difference distributions $\psi(x^*)$, influences of plates behave differently. In the upstream side, the distance from the plate where the effects start to be "felt" (inflection point) does not change with the plate's location. This is the same for both heaving and torsional motions. From the inflection point on, distributions get softened. When the plate is reached, a separation point is provided, the flow is accelerated and the tendency gets broken. Downstream of the vertical plate, this acceleration is translated into a "jump" to the negative side of the phase difference distribution $\psi(x^*)$. The magnitude of this jump varies with the configurations, which means that it is influenced by location of vertical plate. Downstream of the negative peak promoted by the jump, phase difference $\psi(x^*)$ distributions tend to gradually recover positive values.

The increase of the size of the plate enhances the effects on the unsteady pressure characteristics. Although some dependence on the location of the plate can be identified, results show same general tendencies for both sizes. As plate moves to downstream and its size increases, amplitude and phase difference distributions follow opposite tendencies. The influences of the vertical plate on amplitude distributions $\tilde{C}_p(x^*)$ decrease with the increase of its distance from leading edge. This is the opposite of what is observed in phase difference distributions $\psi(x^*)$. Increasing of size of plate enhances this disparity.

A larger size of plate enhances the effects on phase difference distributions $\psi(x^*)$. The "jump" reaches higher values and there is an increase in the distance where the influence of the vertical plate starts to be felt upstream. Downstream of the vertical plate, the recovering tendency is softened and the negative values induced by the vertical plate are kept for longer distances.

(3) Two vertical plates along the chord direction

Further comparisons can be established by checking the effects of two vertical plates of same size installed along chord direction. Vertical plates of sizes *A* and *B* were arranged according set-up *V*. The unsteady pressure characteristics of the resulting configurations, *NF-V-A* and *NF-V-B*, are superimposed in Fig.9 for *U/f.B=25*, along with data from model *NF*. The effects obtained are similar for both sizes and follow similar tendencies as described in the previous section.
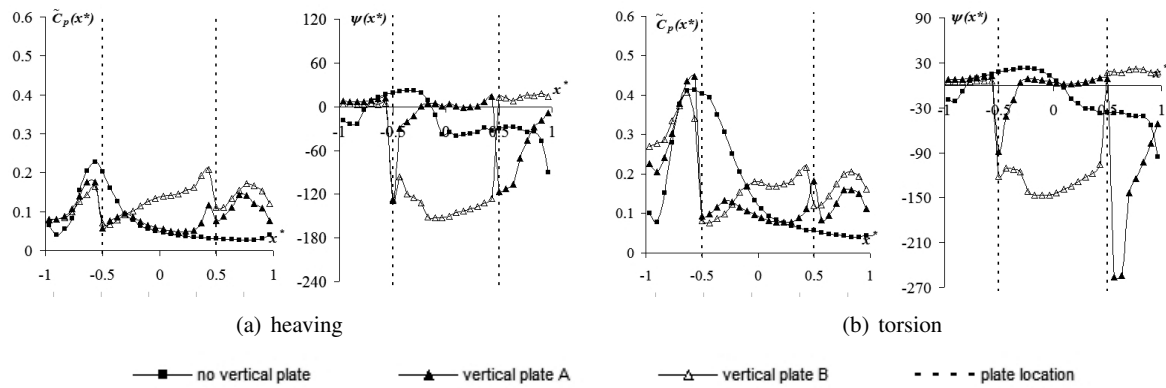

Figure 9: Unsteady pressure characteristics of NF-V-A and NF-V-B at U/f.B=25

Upstream of the plate corresponding to set-up *VI*, both amplitude $\tilde{C}_p(x^*)$ and phase difference $\psi(x^*)$ distributions of set-up *V* behave essentially as they do for case *NF-IV* (Fig.8). Effects of the plate of size *A* corresponding to set-up *VI* on its upstream are practically imperceptible. In the case of plate of size *B*, effects upstream are slightly noticeable. The blockage effect causes an increase in the values of the amplitude $\tilde{C}_p(x^*)$ and the maintenance of the positive values of $\psi(x^*)$. Downstream of the plate corresponding to set-up *VI*, the unsteady pressure characteristics of set-up *V* are similar to those of set-up *VI* itself (Fig.8). As a result, the unsteady pressure characteristics of set-ups *NF-V* become a composition of effects of set-ups *NF-IV* and *NF-VI*, as if both configurations are obtained separately. They can be described as a non cumulative superposition of effects of cases *NF-IV* and *NF-VI*. Such a feature is confirmed from Fig.10.

This is an important characteristic of the compositions of vertical plates studied herein. There seems not to exist a strong interaction between the individual effects of each plate. The unsteady pressure character-
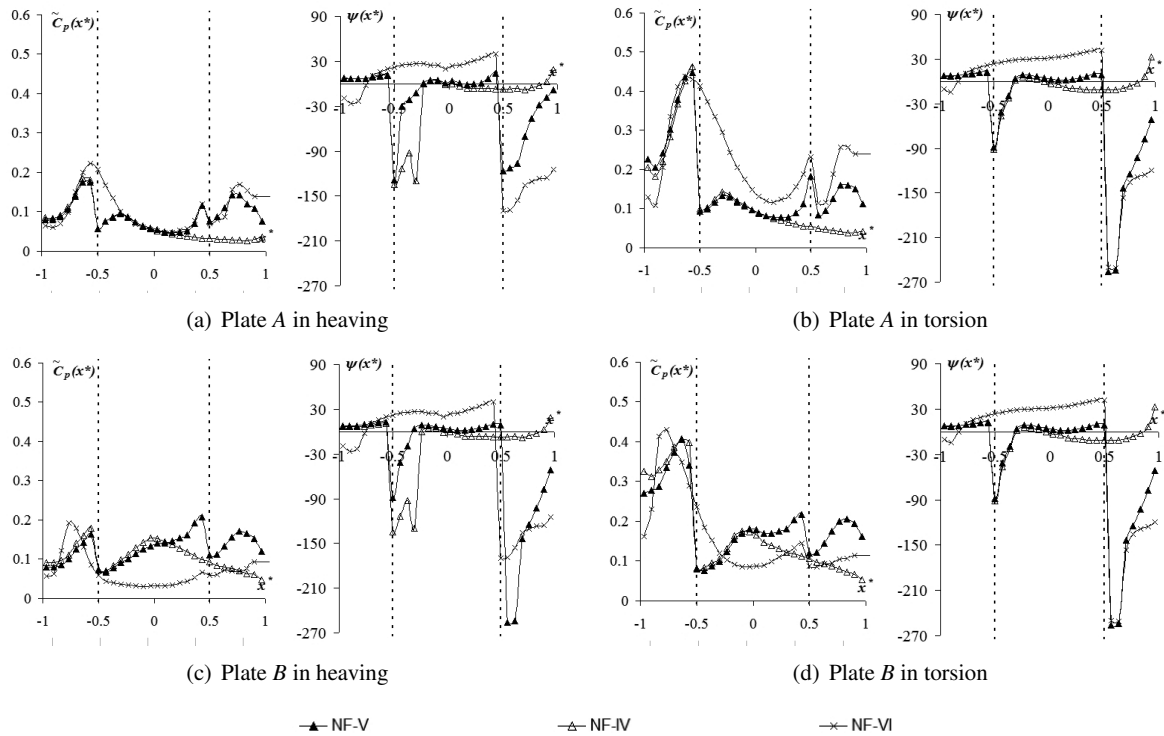
(a) Plate *A* in heaving

(b) Plate *A* in torsion

(c) Plate *B* in heaving

(d) Plate *B* in torsion

Figure 10: Superimposition of the unsteady pressure characteristics for plates *A* and *B* at U/f.B=25

istics downstream of a plate are determined, basically, by only that plate itself, which has little influence on its upstream. Similar effects were observed in two-box configurations[7], which point out a way towards the manipulation of unsteady pressure characteristics.

4. CONCLUDING REMARKS

Effects of vertical plates on the unsteady pressure characteristics of B/D=20 rectangular cylinders were investigated. Vertical plates were found to exert influences not only downstream of their locations, but also upstream, due to the recirculation of the flow caused by a blockage effect. By changing the location of plates was possible to provide plates with different oncoming flow conditions. The resulting effects on the unsteady pressure characteristics varied with such modifications. As a conclusion, influences of plates may be dependent on the characteristics of the flow upstream of their locations. The increase of reduced wind velocity reduced such influences.

Vertical plates were found to induce two peaks in amplitude $\tilde{C}_p(x^*)$ distributions. The first peak occurs at the plate's location and is caused by the blockage of the flow, which is forced to recirculate. The same way that occurs at the leading edge, there is a valley right after the flow separation at the vertical plate. Downstream of the valley, a second peak is promoted, which must be related to flow reattachment. A relationship between size of plate and location of the second peak in amplitude distributions $\tilde{C}_p(x^*)$ could be identified.

As for phase difference $\psi(x^*)$ distributions, a "jump"' is promoted at plate's location, aligned with the first peak in amplitude distribution. Peaks in amplitude distributions $\tilde{C}_p(x^*)$ got reduced with the increase of the distance from leading edge, contrarily to what was observed in phase difference distributions $\psi(x^*)$. The increase of the size of plate enhanced this opposition. When the plate was close enough to the leading edge, effects of both leading edge and plate got superimposed.

In compositions with two vertical plates, there seems to exist a superposition of effects of the both plates. Between the plates, the unsteady pressure characteristics are a composition of the effects obtained separately. Upstream the first plate, unsteady pressure characteristics are similar to those obtained with just that plate. Downstream of the second plate, distributions are influenced, basically, by only that vertical plate itself, regardless the configuration in its upstream.

The combination of all these effects lead to non-linear relationships between size and location of vertical plates and aerodynamic derivatives. Such relationships can be rationalized only by considering the impacts of plates on amplitude and phase difference distributions separately. By doing so, flutter stabilization can be pursued through the proposition of schemes to *manipulate* unsteady pressure characteristics along bridge deck. In this context, the idea of *geometric singularities* was proposed. The concept refers to the insertion of "geometric accidents" along the deck, in proper locations, with the objective of leading phase difference and amplitude distributions to assume configurations suitable for flutter stabilization, according to optimal conditions as discussed in literature[6]. The use of vertical plates in this sense was assessed and attested to be a useful resource.

ACKNOWLEDGEMENTS

REFERENCES

1)   M. Matsumoto, K. Okubo, Y. Ito, H. Matsumiya, and G. Kim. The complex branch characteristics of coupled flutter. *Journal of Wind Engineering and Industrial Aerodynamics*, 96:1843–1855, 2008.

2)   M. Matsumoto, H. Shirato, K. Mizuno, R. Shijo, and T. Hikida. Flutter characteristics of h-shaped cylinders with various side-ratios and comparisons with characteristics of rectangular cylinders. *Journal of Wind Engineering and Industrial Aerodynamics*, 96:963–970, 2008.

3)   X. Chen. Improved understanding of bimodal coupled bridge flutter based on closed-form solutions. *Journal of Structural Engineering*, 60:22–31, 2007.

4)   M. Matsumoto. Aerodynamic damping of prisms. *Journal of Wind Engineering and Industrial Aerodynamics*, 59:159–175, 1996.

5)   R.H. Scanlan, N.P. Jones, and L. Singh. Inter-relations among flutter derivatives. *Journal of Wind Engineering and Industrial Aerodynamics*, 69-71:829–837, 1997.

6)   C. A. Trein and H. Shirato. Coupled flutter stability from the unsteady pressure characteristics point of view. *Journal of Wind Engineering and Industrial Aerodynamics*, 99:114–122, 2011.

7)   C. A. Trein, H. Shirato, and M. Matsumoto. On the effects of the gap on the unsteady pressure characteristics of two-box bridge girders. *Engineering Structures*, 82:121–133, 2015.

8)   C. A. Trein, H. Shirato, and M. Matsumoto. On the unsteady pressure characteristics of modified rectangular cylinders. *Proceedings of VII Asian Pacific Conference on Wind Engineering - APCWE-VII*, 2009.

9)   C. A. Trein, H. Shirato, and M. Matsumoto. Semi-empirical evaluation of the unsteady pressure characteristics of bluff bodies. *Journal of Wind and Engineering*, 7-2:28–38, 2010.

10) C. A. Trein, H. Shirato, and M. Matsumoto. On the effects of the leading edge on the unsteady pressure characteristics of rectangular cylinders. *14th International Conference on Wind Engineering - ICWE14*, 2015.

11) M. Matsumoto, Y. Kobayashi, and H. Shirato. The influence of aerodynamic derivatives on flutter. *Journal of Wind Engineering and Industrial Aerodynamics*, 60:227–239, 1996.

12) M. Matsumoto, F. Yoshizumi, T. Yabutani, K. Abe, and N. Nakajima. Flutter stabilization and heaving-branch flutter. *Journal of Wind Engineering and Industrial Aerodynamics*, 83:289–299, 1999.

13) M. Matsumoto, T. Hikida, and K. Mizuno. On improvement of flutter stability for long-span bridge girders - the case of separated box girders. *Flow Induced Vibration*, 2004.

14) P. J. Saathoff and W. H. Melbourne. The generation of peak pressures in separated/reattaching flows. *Journal of Wind Engineering and Industrial Aerodynamics*, 32:121–134, 1989.